JGR Oceans

RESEARCH ARTICLE
10.1029/2023JC019892

The Combined Effects of Ocean Acidification and Respiration on Habitat Suitability for Marine Calcifiers Along the West Coast of North America

Richard A. Feely[1], Brendan R. Carter[1,2], Simone R. Alin[1], Dana Greeley[1], and Nina Bednaršek[3]

[1]NOAA Pacific Marine Environmental Laboratory, Seattle, WA, USA, [2]University of Washington, Cooperative Institute for Climate, Ocean, and Ecosystem Studies, Seattle, WA, USA, [3]Cooperative Institute for Marine Ecosystem and Resources Studies, Newport, OR, USA

Key Points:

- In the California Current Ecosystem the anthropogenic carbon (C_{anth}) uptake rate at the surface ranges from 0.8 to 1.1 μmol kg^{-1} yr^{-1}
- This corresponds to a total pH decrease of about 0.002 yr^{-1}, whereas the decrease in aragonite saturation ranges from 0.006 to 0.011 yr^{-1}
- Dissolved oxygen consumptions required to cross critical biological thresholds are significantly lower in 2021 than in the pre-industrial

Correspondence to:
R. A. Feely,
richard.a.feely@noaa.gov

Citation:
Feely, R. A., Carter, B. R., Alin, S. R., Greeley, D., & Bednaršek, N. (2024). The combined effects of ocean acidification and respiration on habitat suitability for marine calcifiers along the west coast of North America. *Journal of Geophysical Research: Oceans*, *129*, e2023JC019892. https://doi.org/10.1029/2023JC019892

Received 19 APR 2023
Accepted 10 FEB 2024

Author Contributions:
Conceptualization: Richard A. Feely, Brendan R. Carter
Data curation: Dana Greeley
Formal analysis: Richard A. Feely, Brendan R. Carter, Dana Greeley, Nina Bednaršek
Funding acquisition: Richard A. Feely
Investigation: Richard A. Feely, Nina Bednaršek
Methodology: Richard A. Feely, Brendan R. Carter
Project administration: Richard A. Feely, Nina Bednaršek
Supervision: Richard A. Feely, Nina Bednaršek
Validation: Richard A. Feely, Nina Bednaršek
Visualization: Richard A. Feely, Brendan R. Carter, Dana Greeley

Abstract The California Current Ecosystem (CCE) is a natural laboratory for studying the chemical and ecological impacts of ocean acidification. Biogeochemical variability in the region is due primarily to wind-driven near-shore upwelling of cold waters that are rich in re-mineralized carbon and poor in oxygen. The coastal regions are exposed to surface waters with increasing concentrations of anthropogenic CO_2 (C_{anth}) from exchanges with the atmosphere and the shoreward transport and mixing of upwelled water. The upwelling drives intense cycling of organic matter that is created through photosynthesis in the surface ocean and degraded through biological respiration in subsurface habitats. We used an extended multiple linear-regression approach to determine the spatial and temporal concentrations of C_{anth} and respired carbon (C_{bio}) in the CCE based on cruise data from 2007, 2011, 2012, 2013, 2016, and 2021. Over the region, the C_{anth} accumulation rate increased from 0.8 ± 0.1 μmol kg^{-1} yr^{-1} in the northern latitudes to 1.1 ± 0.1 μmol kg^{-1} yr^{-1} further south. The rates decreased to values of about ~0.3 μmol kg^{-1} yr^{-1} at depths near 300 m. These accumulation rates at the surface correspond to total pH decreases that averaged about 0.002 yr^{-1}; whereas, decreases in aragonite saturation state ranged from 0.006 to 0.011 yr^{-1}. The impact of the C_{anth} uptake was to decrease the amount of oxygen consumption required to cross critical biological thresholds (i.e., calcification, dissolution) for marine calcifiers and are significantly lower in the recent cruises than in the pre-industrial period because of the addition of C_{anth}.

Plain Language Summary The combined effect of ocean acidification and respiration in the California Current Ecosystem is to reduce water column pH and aragonite saturation state, resulting in a compression of the overall size of suitable habitat for marine calcifiers. The addition of excess anthropogenic CO_2 also makes it more likely that critical biological thresholds are crossed and shell dissolution begins to occur. Consequently, the addition of the excess CO_2 also has the added effect of reducing the amount of biological consumption of oxygen that is required to drop the ecosystem below these thresholds.

1. Introduction

Since the start of the industrial era the global oceans have absorbed approximately 170 ± 20 Pg C as carbon dioxide (CO_2), which is roughly 23%–32% of the total amount of CO_2 that has been released into the atmosphere by the combined impacts of human activities (Friedlingstein et al., 2020, 2022; Gruber et al., 2019). This anthropogenic CO_2 (C_{anth}) enters the surface ocean through air-sea exchange where it reacts with seawater to form carbonic acid. Dissociation of carbonic acid then increases the hydrogen ion concentration of seawater in a process known as ocean acidification (OA; Caldeira & Wickett, 2003). Over the timeframe of the industrial era, surface ocean pH has decreased by about 0.11, which is an increase of about 30%–40% in the hydrogen ion concentration (Jiang et al., 2019). Current model projections suggest that by 2100 the pH of surface water is expected to decrease by as much as 0.3–0.4 (IPCC, 2013; Jiang et al., 2019; Joos et al., 2011), and carbonate ion content ($[CO_3^{2-}]$) is expected to decrease as well (Byrne et al., 2010; Feely et al., 2009; Laruelle et al., 2018; Lida et al., 2020; Orr et al., 2005), Consequently, the ocean's capacity to absorb additional amounts of C_{anth} will continue to decline as CO_3^{2-} is depleted (Fassbender et al., 2018; Jones et al., 2013; Kwiatkowski & Orr, 2018; Wang et al., 2017). As a result, the saturation state of aragonite (Ω_{ar}) and calcite (Ω_{cal}); defined as Ω; where $\Omega = [Ca^{2+}][CO_3^{2-}]/K_{sp}^*$, is a function of the concentrations of calcium $[Ca^{2+}]$, carbonate $[CO_3^{2-}]$, and the pressure-dependent stoichiometric solubility product, K_{sp}^* (Mucci, 1983) biogenic mineral phases are diminished. The carbonate saturation state will continue to

Writing – original draft: Richard A. Feely, Brendan R. Carter, Nina Bednaršek
Writing – review & editing: Richard A. Feely, Brendan R. Carter, Simone R. Alin, Nina Bednaršek

decrease as more CO_2 is taken up by the oceans. Thermodynamic equilibrium of the carbonate minerals with the surrounding seawater is reached when $\Omega = 1$. At $\Omega > 1$, precipitation or preservation of carbonate minerals is thermodynamically favored. At or near $\Omega < 1$, net dissolution is generally favored. Global biogeochemical models indicate that with continued atmospheric CO_2 absorption, the ocean is likely to experience declines in calcium carbonate saturation state (Joos et al., 2011; Steinacher et al., 2009). Quantifying C_{anth}, pH, aragonite, and calcite saturation states and rates of change provide a foundation for delineating the tolerance levels of calcifying marine organisms, which evolved over hundreds of thousands of years prior to the influence of human-caused CO_2 emissions.

Recent modeling studies of the California Current Ecosystem (CCE) indicate that the waters along the west coast of North America will experience expanded undersaturated seawater conditions with increasing frequency over the next several decades (Booth et al., 2012; Chan et al., 2017; Desmet et al., 2022; Fassbender et al., 2011; Gruber et al., 2012; Hauri et al., 2013; Siedlecki et al., 2021; Turi et al., 2016). The development of extensive regions of undersaturated water could have profound consequences for marine life and the ecosystem services they provide (Doney et al., 2009, 2020; Ekstrom et al., 2015; Somero et al., 2016). The results for the responses already observed in the CCE show that impaired responses include reduced calcification, slower growth, and thinning of the shells (Mekkes et al., 2021; Osborne et al., 2019), and, depending on the saturation state, substantial dissolution of the aragonite or calcite calcium carbonate ($CaCO_3$) biogenic shells (Bednaršek et al., 2020 and references therein; Feely et al., 2016), as well as physiological stress (Bednaršek et al., 2019; Engström-Öst et al., 2019; Frieder et al., 2014; Gattuso et al., 2015; Somero et al., 2016; Waldbusser et al., 2015) that can in time result in population-level effects, especially in combination with multiple stressors (Bednaršek et al., 2022).

However, current impacts of multiple stressors are still poorly understood, particularly with respect to responses of the calcifiers and their corresponding habitat reduction in the CCE. Conceptually, low CO_2/high Ω_{ar}/high pH with high DO in the preindustrial era allowed for full aerobic performance under the normocapnic conditions, while intensifying OA (high CO_2/low Ω_{ar})/low pH) combined with lower oxygen (DO) reduces organism's aerobic scope, which is a proxy for surplus energy available for vital processes, including growth, reproduction, predator avoidance, etc. (e.g., Pörtner, 2012). The addition of C_{anth} increases CO_2 concentrations (Arroyo et al., 2022) and enhances the intensity and duration of undersaturated conditions for both aragonite and calcite, as well as lower pH levels (Feely et al., 2016). Such exposure has a potential to induce important synergistic interactions (Gobler & Baumann, 2016). Resolving how reduced suitable habitat conditions change the fitness of marine calcifiers within the CCE is possible though the applications of essential biological thresholds that exist for various functional groups (Bednaršek et al., 2019, 2020, 2021).

The California Current is a southward flowing eastern boundary current that encompasses the region off west of Vancouver Island in Canada to the coastal waters off southern California and northern Mexico (Figure 1). The coastal waters shoreward of the California Current experience strong seasonal upwelling from early spring to early fall. The upwelling is due to changes in the position of the high-pressure atmospheric cells that cause the strengthening of northwesterly winds that drive surface water offshore via Ekman transport and induce the upwelling of low pH, and nutrient- and CO_2-rich, intermediate depth (150–300 m) offshore waters onto the continental shelf as a component of the California Undercurrent (Feely et al., 2008; Grantham et al., 2004; Gruber et al., 2012; Hales et al., 2005, 2006; Harris et al., 2013; Hauri et al., 2013; Rykaczewski & Dunne, 2010; Thomson & Krassovski, 2010; Turi et al., 2016). The upwelling occurs from spring to early- or mid-fall. Within the CCE, the upwelling supports high amounts of primary production on the continental shelf and slope. While upwelling plays a defining role in CCE biogeochemistry, productivity, and ecology, it also contributes to local and regional oceanographic processes that enhance the effects of ocean acidification. The waters that are undersaturated with respect to aragonite ($\Omega_{ar} < 1$) or calcite ($\Omega_{cal} < 1$) biogenic mineral phases are the result of the combined processes of: (a) oceanic uptake of anthropogenic CO_2, and (b) the build-up of CO_2 from the natural respiration processes that are enhanced on the continental shelf after the interior waters have upwelled.

In this paper, we estimate the rates of C_{anth} accumulation and decrease in Ω_{ar} and pH in the CCE region from data obtained on cruises from 2007 through 2021 and delineate the carbonate chemistry changes with a goal of providing a better understanding of the interactions between ocean acidification and respiration and their implications for associated biological OA-related thresholds for current and preindustrial conditions.

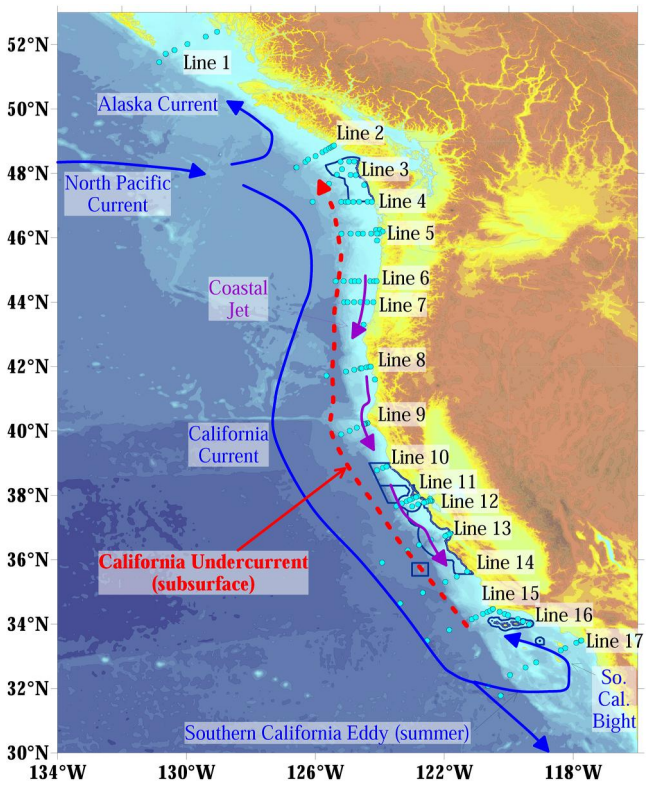

Figure 1. Map of the station locations for the 2021 West Coast (WCOA2021) cruise. The section line names are positioned next to each station transect. The 2007, 2011, 2012, 2013, and 2016 cruises had similar station spacings stretching from Canada to Baja California, Mexico.

2. Analytical Methods for the Analysis of the Observations

2.1. Chemical Methods

In the late spring of 2007 and 2016 and during the summers of 2011, 2012, 2013, and 2021 we conducted detailed observations of carbon system chemistry and other physical, chemical, and biological measurements along the western North American continental shelf (Figure 1). Water samples from the cruises were collected in modified Niskin-type bottles and analyzed under laboratory conditions for dissolved inorganic carbon (DIC), total alkalinity (TA), oxygen, and nutrients. DIC was analyzed using coulometric titration (DOE, 1994; Johnson et al., 1987; Ono et al., 1998). TA was measured by the open cell potentiometric titration method with a low (~3.5) pH endpoint (DOE, 1994; Millero, 1995; Millero et al., 1993; Ono et al., 1998).

Using the measurements of Certified Reference Materials (DOE, 1994) as independent checks on our standards returned DIC and TA values that were within ±2 μmol kg^{-1} of the certified values. Consequently, no CRM corrections were applied to the data sets. Replicate analysis of samples confirmed strong short-term repeatability such that the ship-based DIC and TA data are both precise to within ±2 μmol kg^{-1}. The aragonite and calcite saturation states of seawater were calculated from the DIC and TA data using the program CO2SYS developed by Lewis and Wallace (1998), using the constants of Lueker et al. (2000) for carbonate speciation, Dickson (1990) for the [HSO_4^-] speciation, and Lee et al. (2010) for total boron based on salinity. The pressure effect on the solubility, for samples collected at depth, is estimated from the equation of Mucci (1983), incorporating adjustments to the constants recommended by Millero (1995). Based on the uncertainties in the DIC and TA measurements and the thermodynamic constants, the uncertainty in the calculated Ω_{ar} is approximately 0.02. Oxygen analysis was conducted by modified Winkler titration (Carpenter, 1965), and nutrients (nitrate, nitrite, ammonium, phosphate, silicate) were analyzed using a Technicon AutoAnalyzer II (UNESCO, 1994).

2.2. Determination of Anthropogenic Carbon Dioxide and Re-Mineralized Carbon

Anthropogenic carbon (C_{anth}) accumulation was estimated using the approach outlined by Carter et al. (2017, 2019) and refined in Arroyo et al. (2022). This approach is based on calculations obtained by combining the apparent decadal accumulation of anthropogenic carbon since 1994 assessed by applying a modified version of the extended multiple linear regression method (Friis et al., 2005) to data from 14 repeatedly measured Pacific hydrographic transects with the ΔC*-based estimates of C_{anth} in 1994 provided by Sabine et al. (2004). The C_{anth} estimates, which are scattered both temporally and spatially, are then re-mapped to observed physical properties by fitting a Locally Interpolated Regression (LIR) that reconstructs the estimates based on observed temperature, salinity, depth, latitude, longitude, and year. The only deviations from the LIR-fitting methods outlined by Carter et al. (2019) were that the latitude, longitude, and depth/density restriction windows used for selecting subsets of the data for regression were removed and the weighting term (their equation 3) was squared. Previously, the LIR used restrictive depth windows for data selection and the corresponding approximated spatiotemporal objective mapping routine appropriate for basin-scale inventory change estimates. However, the squared weighting term has subsequently been shown to be effective at ensuring that the regression coefficients remain local even in the absence of data in the selection windows. Importantly, as modified, the LIR coefficients have stronger dependencies on temperature and salinity (and weaker dependencies on depth), which is appropriate for mapping the variations over time in the presence of intense coastal upwelling. This approach represents an improvement over the approach used previously by Feely et al. (2016) due to the larger quantities of C_{anth} estimates used to fit the relationships used to quantify C_{anth}; that is, the Feely et al. (2016) paper fit second order polynomials to C_{anth} estimates from a single zonal (P02) and a single meridional (P16) section intersecting the North American Coast within the CCE and the Gulf of Alaska, respectively, whereas the new approach use these sections along with

Table 1
Average and Root Mean Square Differences Between the C_{anth} Estimation Used in This Paper and the Approach Used by Feely et al. (2016) Polynomial (This Study Minus "Feely et al., 2016")

Dataset year	Average offset (μmol kg^{-1})	Root mean square difference (μmol kg^{-1})
2007	−1.3	4.9
2011	−3.2	6.1
2012	−3.9	6
2013	−4.1	6.4
2016	−4.9	7.3
2021	−3	8.9

many additional sections and directly incorporates anthropogenic change estimates derived from the 2007 to 2021 WCOA cruise occupations (Carter et al., 2019). Despite the change in the methods, the new approach does not yield significantly different C_{anth} estimates on average (Table 1), suggesting that both approaches are comparable to within the previously stated standard uncertainties of ∼8 μmol C_{anth} kg^{-1} (Feely et al., 2016).

We estimate C_{bio}, or the amount of additional DIC present resulting from organic matter remineralization from seawater and root mean properties using the methods described in Feely et al. (2016), where C_{bio} is estimated by multiplying the apparent oxygen utilization—or the oxygen concentration at saturation minus the observed oxygen concentration determined by the remineralization ratio relating oxygen and inorganic carbon (117/170), as given in Anderson and Sarmiento (1994). In the surface ocean, C_{bio} represents air-sea disequilibria that are primarily from net photosynthesis (negative values) or net respiration (positive values) or from recent upwelling of deeper waters that have experienced these processes. These disequilibria are abated over time by gas exchange of O_2 and the C_{bio} estimate will be an underestimate in many instances because the O_2 air-sea equilibration occurs more rapidly than disequilibria in CO_2 system variables. With the added complexity of air-sea gas exchange timescales, these estimates are challenging to interpret within the surface mixed layers, but nevertheless important to present as an indicator of short-timescale surface variability. The calculations reported in Table 1 are for broad regions of the US West Coast using temperature, salinity, and oxygen values measured on WCOA cruises and gridded for the continental shelf (defined as areas with bathymetric depths of 200 m or less). All data were used for the gridding, which was performed using 3D linear triangulation with latitude, depth, and bathymetric depth as gridding coordinates following the procedures outlined by Feely et al. (2016).

2.3. Biological Examinations

2.3.1. Determining Pteropod Shell Dissolution

Pteropod samples were collected in 333 μm Bongo nets towed for 30 min on oblique tows from 100 m to the surface and preserved in 90% buffered ethanol prior to analysis by scanning electron microscopy. For pteropod shell dissolution, a well-known and used scheme for categorizing dissolution into three types of dissolution exists (Bednaršek et al., 2012). The types I, II, III are based on the severity of dissolution and can be easily recognizable and distinguished on the SEM images of each pteropod shell. This study focused on the extent of Type II and Type III dissolution of *L. helicina* pteropod shells following the approach described in Bednaršek et al. (2020). Type II and Type III dissolution are determined as severe dissolution, in which the occurrence (presence or absence) on the shell was a critical criteria for determining whether the shell was then counted toward the number of individuals affected by severe dissolution. Shell dissolution was not quantified on the individual pteropod level, rather we focused on counting the pteropods with severe dissolution in a sample. Only one person analyzed all the pteropod images, so there was no bias toward analyzing the images. In addition, the station samples were station-blinded before the analyses to remove any potential bias.

2.3.2. Application of OA-Related Thresholds

The threshold for the CCE-related species for pteropods, decapods and echinoderms for the CCE have been selected through an expert consensus process based on previously published results in Bednaršek et al. (2019, 2020, 2021). We applied several of these thresholds pertaining to the vital pelagic biological processes for

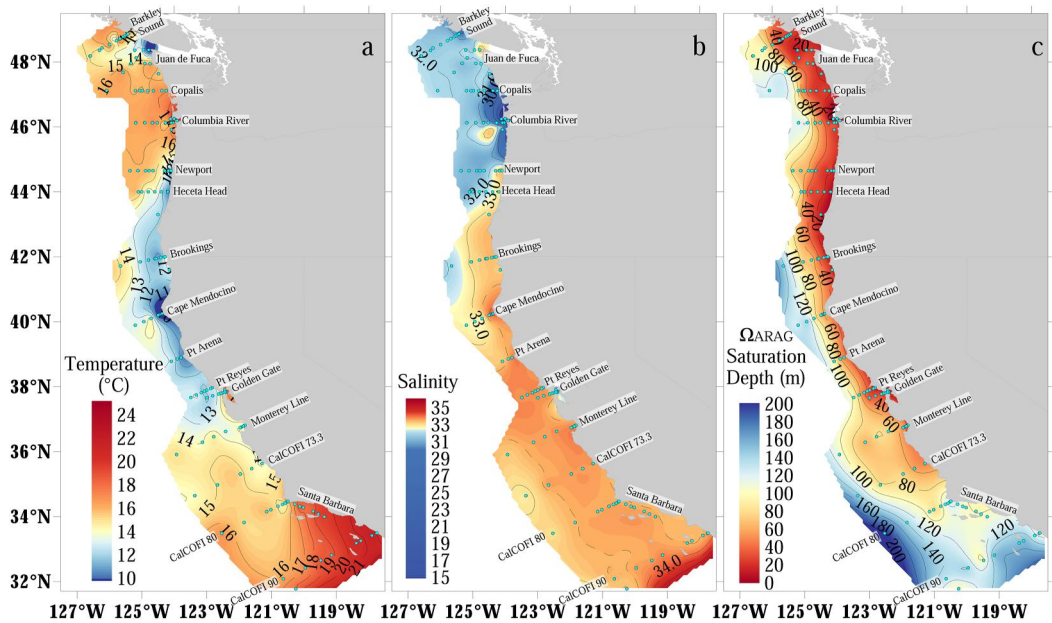

Figure 2. Surface distribution of: (a) temperature; (b) salinity; and (c) aragonite saturation depth along the coastal margin of the CCE during the WCOA2021 cruise in June–July.

pteropods (survival, severe dissolution, calcification): decapods (growth and hatching) and larval stages of echinoderms (swimming and growth (development, survival, calcification) to conceptually investigate the changes in their habitat since the pre-industrial time.

3. Results

3.1. Distribution of Temperature, Salinity, and Aragonite Saturation Depth in 2021

During the WCOA 2021 and earlier cruises, the surface waters were characterized by increasing north to south temperature values ranging from about 11 to 16°C in the coastal waters north of Point Reyes, CA, compared with 14–22°C in the southern California coastal waters. Low surface water temperature values (<12°C) were observed near the coast off Oregon south of Newport and just off the northern and central California coast due to strong coastal upwelling that brings cold CO_2-rich waters to the surface (Figure 2a) and spreads out over the shelf.

The range of measured salinity values is from approximately 3 to 35. Salinity also shows an increasing trend from north to south, and throughout the northern part the region there is also a general increasing onshore-offshore trend due to freshwater input and mixing along the coast (Figure 2b). Off Cape Mendocino the salinity values are generally higher and more uniform due to the coastal upwelling of higher salinity subsurface waters. The lowest salinity waters are observed within the region of the Columbia River mouth and in the nearshore waters off Vancouver Island where estuarine circulation in the near-surface waters contribute to the lower salinity. The highest salinities occur in the southern California waters and in the Baja California coastal waters based on the earlier cruise in 2007 and 2016 (data not shown in Figure 2).

The depth where $\Omega_{ar} = 1.0$, or the so-called "aragonite saturation horizon," is generally at about 80–160 m near the shelf break. From there it tends to slope upward toward the coast, reaching depths as shallow as 20–40 m near the coast in the northern part of the study region compared with 50–160 m near the coast in the southern half of the study region (Figure 2c).

3.2. Rates of Change of Anthropogenic CO_2, pH, and Aragonite Saturation State

The six coastal cruises were occupied during the spring (2007, 2016) and summer (2011, 2012, 2013, and 2021) months where the impacts of upwelling were observed in the section plots (not shown) within the nearshore regions off Vancouver Island, Canada to off Baja California, Mexico. The results indicate significant large-scale

Table 2
Average Anthropogenic Carbon (C_{anth}) and Remineralized Carbon (C_{bio}) Estimates in Coastal Waters Shallower Than 200 m Depth

		0–10 m depth		50–55 m depth		90–100 m depth	
Region	Year	^{C}anth	^{C}bio	^{C}anth	^{C}bio	^{C}anth	^{C}bio
W	2007	48.9	−27.4	38	84.4	34.8	130.9
W	2011	50.9	96.9	39.3	124.7	36.7	148.1
W	2012	55.2	85	39.2	118.1	37.3	149.2
W	2013	50.9	45.3	39.4	110	37.2	151.8
W	2016	58.6	−43.8	45.4	99.9	41.5	125.6
W	2021	73.3	−39.6	45.2	130.6	41.7	165.5
O	2007	48.1	21.8	38.9	93.1	36	147.1
O	2011	49.6	33.6	40.1	114.6	38.3	158
O	2012	52.8	18.6	42	88.2	40.2	132
O	2013	54.6	39.3	41.6	121.8	39.7	150.4
O	2016	59.9	−19.5	46.8	101.1	42.9	134.2
O	2021	69.6	−11.5	46.9	131.8	44.7	163
NC	2007	38.1	32.4	35.3	96	33	135.1
NC	2011	50.4	48.9	43.1	107.7	41	137.4
NC	2012	53.3	27.7	45.9	81.6	43.9	112.3
NC	2013	54.2	16.9	44.9	96.7	41.9	136.9
NC	2016	52.6	23.2	45.2	101	41.4	131.7
NC	2021	59.7	14.6	49.7	111	47.1	131.3
SC	2007	54.4	−22.8	38.1	117.3	35.2	135.3
SC	2011	56.6	24	46.7	50.6	43.2	77.5
SC	2016	62.4	8	50.6	80.4	44.5	115.5
SC	2021	77.6	−13.8	55.6	63.6	49.4	101
Average		56	16	44	101	41	135

Note. Estimates are averaged by region (W: Washington, O: Oregon, NC: Northern California, SC: Southern California) for the 3 different depth ranges indicated. Concentrations are in units of μmol kg^{-1}.

horizontal and vertical concentration gradients of C_{anth} in surface and subsurface waters. This is due to local exchanges with the atmosphere and the shoreward transport at depth and mixing of upwelled water from the open-ocean intermediate depths along the shelf-slope boundary to the bottom waters on the shelf (Table 2). Concentrations of C_{anth} in surface waters not affected by strong upwelling ranged from 48 μmol kg^{-1} in the northern surface waters in 2007 to about 78 μmol kg^{-1} in the southern surface waters off the coast of California in 2021 (Figures 3a and 3b). A large part of these differences is due to the increase in C_{anth} with time over the duration of the cruises. However, some portion of this difference may be due to the increasing buffering capacity in the warmer, high salinity waters to the south. In the upwelled waters off Cape Mendocino C_{anth} values at the surface were as low as 38 μmol kg^{-1} in 2007, reflecting the upwelling of older subsurface water from deeper depths in this region.

During the earlier cruises surface water C_{anth} concentrations were lower (38–49 μmol kg^{-1}), particularly in the strong upwelling nearshore coastal region close to Cape Mendocino. Over the decade from 2007 to 2016 the C_{anth} accumulation rates in surface waters ranged from 0.8 to 1.1 ± 0.1 μmol kg^{-1} yr^{-1}, with the higher rates in the southern surface waters relative to the north. The C_{anth} accumulation rates gradually decrease with depth to values of ranging from about 0.4 to 0.3 μmol kg^{-1} yr^{-1} at depths near 300 m, with slightly higher rates to north where vertical mixing is stronger. Below about 300–400 m the C_{anth} accumulation rate decreases to values below the detection limit depending on location (Figure 3b).

Table 2 provides the distribution and ranges of remineralized carbon concentrations (C_{bio}) over three depth ranges in several regions of the CCE. Considering average values across the entire US West Coast, C_{bio} concentrations are lowest near the surface where air-sea gas exchange and biological uptake of carbon attenuate C_{bio} accumulation. Negative values in the surface mixed layer are indicative of supersaturated waters with respect to dissolved O_2. These values are consistent with the higher productivity and, consequently, high variability in near-surface waters and subsequent remineralization of organic matter at depth, particularly in the northern half of the study region (Siedlecki et al., 2016). In subsurface waters, C_{bio} values are more uniform and show the highest values off the coasts of Washington, Oregon, and northern California, ranging from 50 to 170 μmol kg^{-1} in the deeper depths (Figure 4). The variability of C_{bio} in the subsurface waters does not follow the long-term trends of C_{anth}, suggesting that C_{bio} is perhaps more effectively controlled by interannual variations in local respiration processes rather than secular increases in carbon. These biologically-generated additions of dissolved CO_2 combine with the C_{anth} to make up the total enrichment of CO_2 in the subsurface waters, with the highest values generally occurring in the northern waters where primary production and hypoxic conditions are most often observed in mid-shelf and nearshore regions from late spring through early fall months due to the long water mass retention time and enhanced respiration (Alin et al., 2021; Siedlecki et al., 2016).

Since the aragonite saturation state is a function of the total dissolved CO_2, total alkalinity, temperature, salinity and pressure, it is expected that calculated surface water Ω_{ar} values would exhibit a high degree of variability depending on the C_{bio} and C_{anth} concentrations, extent of upwelling, degree of warming, and freshwater input. Accordingly, surface Ω_{ar} values range from 1.0 to 3.0, with the lowest values occurring in the region of the outflow from the Columbia River and in the strong upwelling regions along the Washington, Oregon, and northern California coasts (Figure 5a). Subsurface Ω_{ar} values show evidence for undersaturation at depths ranging from 20 to 100 m in the northern half of the region and 50–160 m in the southern half. The strong north-to-south increase in saturation depth is a function of the increasing water temperature and decreasing DIC from north to south in the subsurface waters (Carter et al., 2017; Jiang et al., 2019). The rate of decrease in aragonite saturation

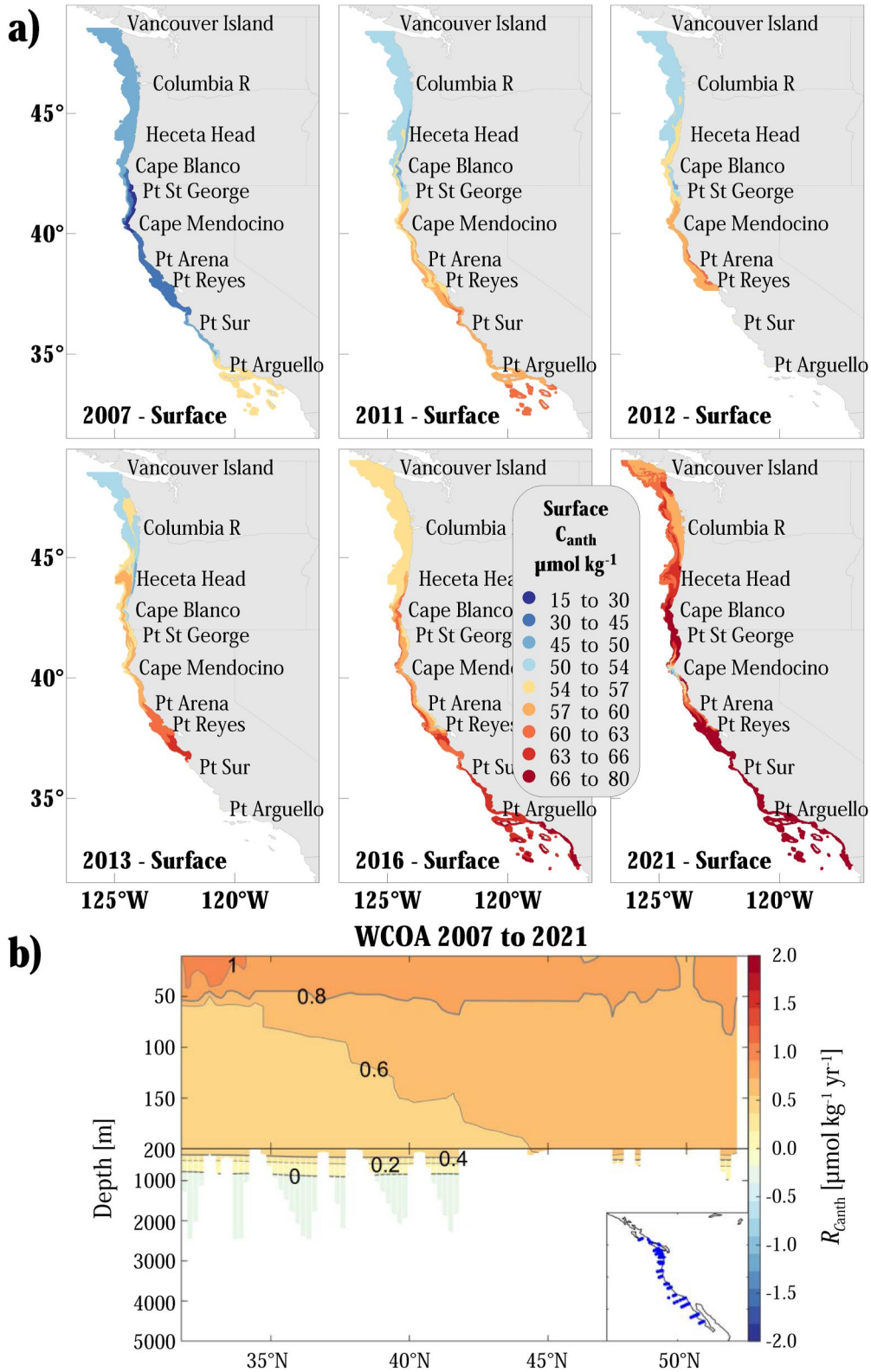

Figure 3. Distribution of: (a) anthropogenic CO_2 (in μmol kg^{-1}) at the surface; and (b) anthropogenic CO_2 rate of change in μmol kg^{-1} yr^{-1} along the coast from south to north. Vertical white lines below ~400 m indicate locations where the accumulation rates in the region are not significantly different from 0.

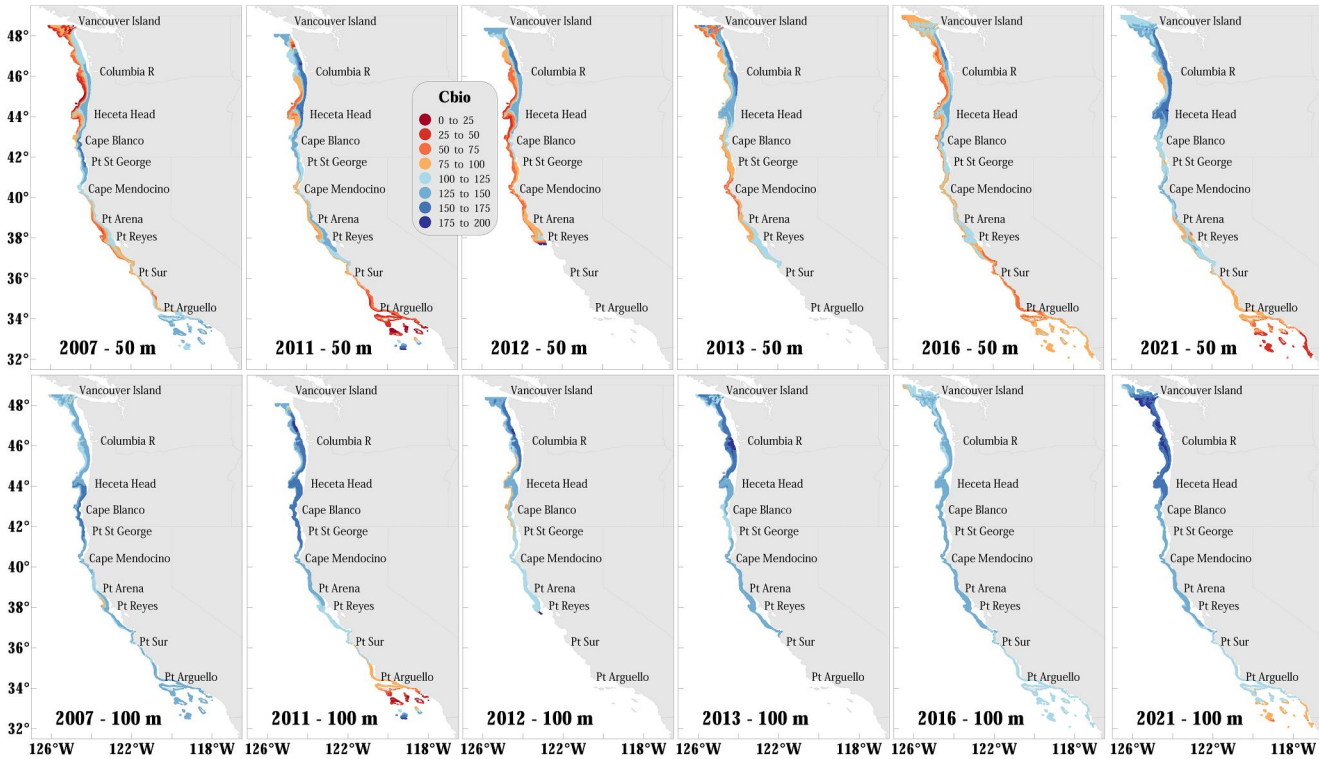

Figure 4. Estimated C_{bio} concentrations in μmol kg^{-1} at 50 m, and 100 m in the continental margin region from Canada to Mexico.

state ranges from 0.006 to 0.011 yr^{-1} in surface waters and drop to values less than 0.002 yr^{-1} below 200 m (Figure 5b).

Surface water pH_T (total scale) distributions exhibited large spatial variability, ranging from 7.7 to 8.3. The lowest pH values were found in the nearshore upwelling regions off the Washington, Oregon, and northern California coasts (Figure 6a). High pH_T values (8.0–8.3) were generally observed in the offshore waters in the northern half of the study area during the spring cruises off Washington and Oregon, consistent with the hindcast model results of Turi et al. (2016). Near the mouth of the Columbia River, surface pH_T values were lower than the surrounding water due to the outflow of low salinity, low alkalinity riverine water in the surface layer (Evans et al., 2013). Over the period from 2007 to 2021 pH_T values decreased by an average of −0.002 yr^1 in the upper 50 m of the water column (Figure 6b), with significant decreases in the rate of pH_T decline at depths down to approximately 300 m north of 40°N.

3.3. Impact on Biogeochemical Processes and Biological Thresholds

To quantitatively understand the impact of C_{anth} and respiration processes on aragonite saturation state, the aragonite saturation state was plotted versus dissolved oxygen for preindustrial and 2021 conditions (Figure 7a). The preindustrial conditions were estimated by subtracting the 2021 C_{anth} concentrations from the DIC values and recalculating the aragonite saturation state using CO2SYS, assuming no substantial change in oxygen concentrations have occurred over that period. The figure indicates a strong nonlinear relationship that can be reasonably approximated with a polynomial function ($R^2 = 0.86$). While there is considerable scatter of the data in surface waters, the slope is strongest in subsurface waters where respiration processes and C_{anth} input are the major causes of the decreasing aragonite saturation state with increasing depth in the water column. Aragonite saturation state drops below the value of 1.0 at an oxygen concentration of approximately 145 μmol kg^{-1} in 2021 and 93 μmol kg^{-1} in the preindustrial period. Thus, the impact of the additional amount of C_{anth} added to the subsurface waters in this region results in conditions that are closer or below the critical thresholds for marine pelagic calcifiers more often at present compared to the pre-industrial times (Table 3), or alternatively, such conditions require less respiration to bring the system below the critical thresholds for marine pelagic organisms. Overall,

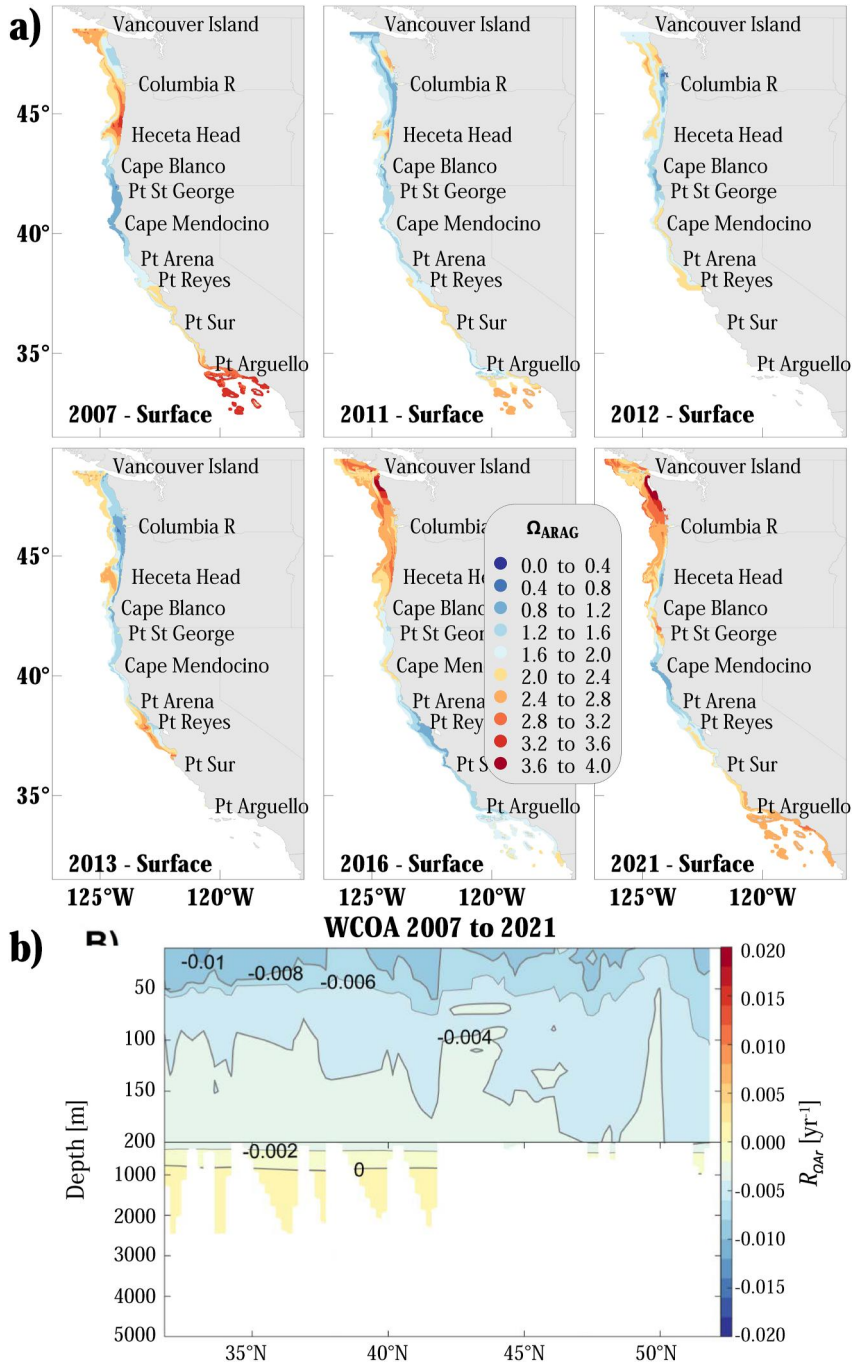

Figure 5. Distribution of: (a) aragonite saturation state, Ω_{ar}, at the surface; and (b) vertical distribution of aragonite saturation state rate of change in the California Current Ecosystem.

this implies reduced volume of suitable habitat, which results in more severity of the biological impairment processes, including survival, biomineralization for pteropods, growth and hatching for decapods, and swimming and growth for echinoderms (Table 3). Consistently across all the thresholds for three functional groups, the conditions are now crossed at much higher DO concentrations compared to the pre-industrial times. For example, for the biological threshold of severe dissolution occurs at the aragonite saturation state of 1.2 and DO of approximately 179 μmol kg^{-1} in 2021, compared to the preindustrial DO of 125 μmol kg^{-1}, amounting to a difference of 54 μmol kg^{-1}. Similarly, pH of 7.8 (threshold for decapod hatching success) is currently crossed at 180 μmol kg^{-1}, while in the preindustrial period this occurred at much lower DO concentration (111 μmol kg^{-1}),

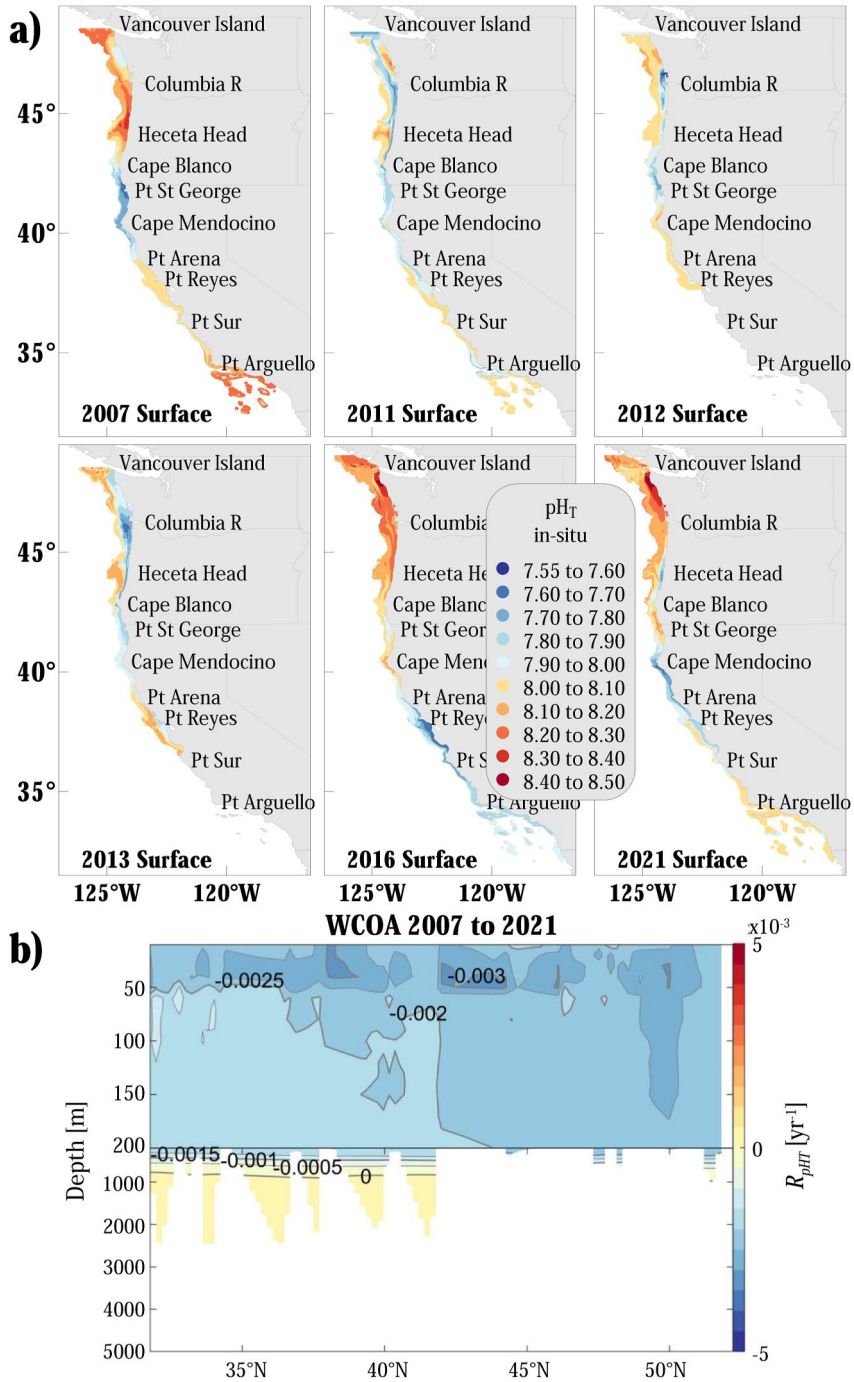

Figure 6. Distribution of: (a) pH_T at the surface; and (b) south to north vertical distribution of pH_T rate of change in the California Current Ecosystem.

with a difference of 71 μmol kg^{-1} (Table 3) or at approximately 40% higher DO. While the results for the higher saturation state threshold follow the same overall trend, the differences are larger when the thresholds occur at higher saturation states, as exemplified in echinoderms, where the thresholds are crossed at 60% higher DO concentrations.

In addition, biological field responses are presented where the chemical and biological samples were co-located during the 2011, 2013, and 2016 cruises. Based on 46 datapoints across the three cruises, the results indicate a strong negative linear correlation between the percentage of individuals with severe dissolution (Type II or

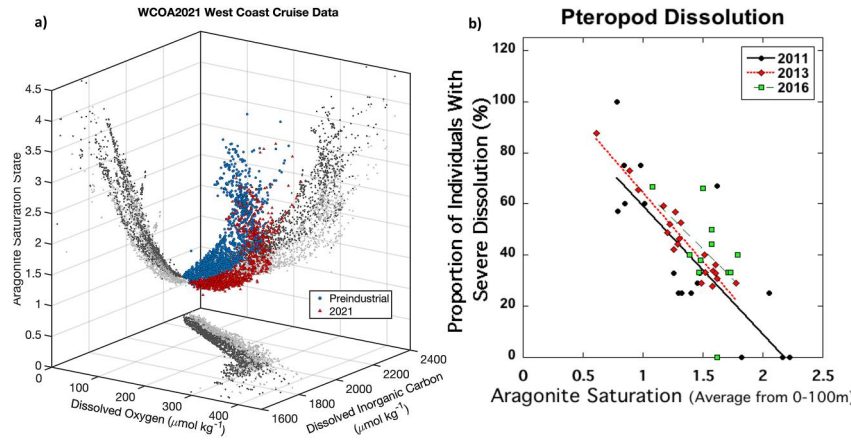

Figure 7. (a) 3-D plot of the relationship between aragonite saturation state versus dissolved oxygen and dissolved inorganic carbon for preindustrial (blue and dark gray dots) and the 2021 observations (red and light gray triangles); and (b) relationship between the proportion of *L. helicina* pteropods that exhibit Type II or Type III dissolution versus aragonite saturation state averaged over the upper 100 m of the water column from the 2011, 2013, and 2016 cruises with linear fit of $y = -49.43x + 112.22$; $R^2 = 0.65$ The threshold for severe dissolution has been determined to be at an aragonite saturation state value ~1.2 based on the expert consensus studies (after Bednaršek et al., 2019). The pteropods that show severe dissolution from the cruise results are primarily from the samples located shoreward of the shelfbreak.

Type III) and aragonite saturation state averaged over the top 100 m (49.43x + 112.22; $R^2 = 0.65$; Figure 7b). The occurrence of mild and severe dissolution metrics are sensitive and reliable indicators of exposure and the potential for sublethal impairment, respectively. Based on laboratory studies, thresholds for mild and severe dissolution (Bednaršek et al., 2019) are crossed upon pteropod exposure range of $1.5 > \Omega_{ar} > 1.2$ for 7–14 days, with such levels of severe dissolution observed in many of the samples. The cruise results indicate that the most severe impacts occur in the on-shelf subsurface waters because this region has the strongest combination of impacts due to C_{anth} inputs and seasonal respiration processes. Additional results from Table 3 for severe dissolution demonstrate that this threshold now requires much higher DO concentrations (i.e., 136 and 145 μmol kg^{-1}) compared to the pre-industrial times (i.e., 85 and 93 μmol kg^{-1}), indicating that these thresholds are crossed higher in the water column and, consequently, resulting in reduced overall volume of suitable habitat for pelagic calcifiers in the upper 200 m.

Table 3
Dissolved Oxygen Concentrations at Thresholds With and Without Anthropogenic CO_2

Threshold	Preindustrial oxygen concentration at threshold (μmol kg^{-1})	2021 oxygen concentration at threshold (μmol kg^{-1})	Difference (μmol kg^{-1})
Threshold for Pteropods			
Aragonite 0.95 – survival	85	136	51
Aragonite 1.0 – thermodynamic	93	145	52
Aragonite 1.2 – severe dissolution	125	179	54
Aragonite 1.25 – impaired	133	187	55
Calcification			
Threshold for Decapods			
pH 7.5 – growth rate	85	158	73
pH 7.8 – hatching success	111	180	71
Threshold for Echinoderms			
pH 7.64 – growth rate	27	101	74
pH 7.70 – swimming rate	59	133	74

Table 4
Rates of DIC, pH, and aragonite Saturation State (Ω_{ar}) Change in Surface Waters of the California Current Ecosystem and Other Locations in the Pacific Ocean

Location	Type of Observations	Study Period	DIC change yr^{-1} µmol kg^{-1} ± 1sd	pH change yr^{-1}	Ω_{ar} change yr^{-1}	Reference
California Current System	Shipboard Observations	2007–2021	0.9 ± 0.1	−0.002 ± 0.0005	−0.007 ± 0.002	This study
California Current System	Shipboard Observations	1993–2018		−0.0024 ± 0.0006		Chavez et al., 2017
California Current System	Shipboard Observations	1983–2021	0.7 ± 0.05	−0.0015 ± 0.0001	−0.0062 ± 0.0008	Wolfe et al., 2023
NP-STPS	Shipboard Observations	1991–2011		−0.0019 ± 0.0002		Lauvset et al., 2015
Northeast Pacific Subarctic Gyre	Shipboard Observations	1990–2020	0.6 ± 0.3	−0.0014 ± 0.0004	−0.005 ± 0.002	Franco et al., 2021
Papa, 50°N, 145°W	Mooring	2007–2014	−1 ± 0.3	−0.001 ± 0.0005	0.01 ± 0.004	Sutton et al., 2017
K2, 47°N, 160°E	Shipboard Time Series	1999–2015		−0.0025 ± 0.001	−0.012 ± 0.005	Wakita et al., 2017
KEO, 32°N, 144°E	Mooring	2007–2014	1.3 ± 0.2	−0.001 ± 0.0005	−0.01 ± 0.002	Sutton et al., 2017
NP-STSS	Shipboard Observations	1911–2011		−0.001 ± 0.0005		Lauvset et al., 2015
HOT, 22.75°N, 158°W	Shipboard Time Series	1988–2011	1.78 ± 0.12	−0.0016 ± 0.0001	−0.0084 ± 0.0011	Bates et al., 2014
WHOTS, 23°N, 158°W	Mooring	2004–2013	1.6 ± 0.2	−0.002 ± 0.0003	−0.02 ± 0.002	Sutton et al., 2017
137°E, 33–34°N	Shipboard Observations	1994–2008	1.2 ± 0.4	−0.002 ± 0.0007	−0.012 ± 0.005	Ishii et al., 2011
137°E, 26°N–30°N	Shipboard Observations	1983–2017	1.2 ± 0.05	−0.0019 ± 0.0008	−0.012 ± 0.005	Ono et al., 2019
137°E, 20°N–22°N	Shipboard Observations	1983–2017	1.1 ± 0.04	−0.0017 ± 0.0007	−0.011 ± 0.004	Ono et al., 2019
137°E, 5°N–10°N	Shipboard Observations	1983–2017	0.8 ± 0.05	−0.0012 ± 0.0008	−0.0081 ± 0.005	Ono et al., 2019
NP-SPSS	Shipboard Observations	1991–2011		−0.0013 ± 0.0005		Lauvset et al., 2015
WP-EQA	Shipboard Observations	1991–2011		−0.0012 ± 0.0002		Lauvset et al., 2015
Warm Pool, 130°E–180°	Shipboard Observations	1985–2016		−0.0013 ± 0.0007	−0.0083 ± 0.0007	Ishii et al., 2020
EP-EQU	Shipboard Observations	1991–2011		−0.0026 ± 0.0002		Lauvset et al., 2015
TAO, 0°, 155°W	Mooring	1997–2011		−0.0022 ± 0.0003		Sutton et al., 2014
TAO, 0°, 140°W	Mooring	2004–2011		−0.0018 ± 0.0004		Sutton et al., 2014
TAO, 0°, 125°W	Mooring	2004–2011		−0.0026 ± 0.0005		Sutton et al., 2014
Munida, 45.833°S, 171.5°E	Shipboard Observations	1998–2011	0.88 ± 0.30	−0.0013 ± 0.0003	−0.0085 ± 0.0026	Bates et al., 2014
SP-STPS	Shipboard Observations	1991–2011		−0.0022 ± 0.0003		Lauvset et al., 2015

4. Discussion

As a direct consequence of the surface ocean uptake of anthropogenic carbon dioxide from the atmosphere, DIC concentrations are increasing along the west coast of North America. To place these changes into a larger oceanographic context the rates of increase in DIC, the decrease in pH_T, and the decrease in aragonite saturation state are compared for the coastal waters of the California Current Ecosystem along the Pacific Coast along with similar calculations for open-ocean and coastal regions in the Pacific Ocean (Table 4). The DIC increase in open-ocean surface waters range from 0.6 to 1.6 µmol kg^{-1} yr^{-1}, with the highest rates of change occurring in the central and western North Pacific subtropical gyre where salinity and buffer capacity are also high (Sabine et al., 2004). The rates of DIC increase in the CCE average about 0.9 ± 0.1, which is consistent with other measurements for the region and slightly lower than the average of the open-ocean values in the central and western North Pacific.

The CCE pH_T changes average about −0.002 ± 0.0005 yr^{-1}, which is slightly higher than the rate of change expected from the air-sea uptake of anthropogenic CO_2 over the last two decades in the Pacific (Table 4). This rate of change is among the highest found in the Pacific and is consistent with other upwelling regions in the tropical Pacific where the lower buffer capacity enhances the pH change in the direction of higher acidity (Feely et al., 2018). The lowest rate of pH change generally occurs in the equatorial and subtropical waters of the western Pacific where the buffer capacity is highest and, consequently, the waters are more resilient to pH change (Egleston et al., 2010; Sabine et al., 2004).

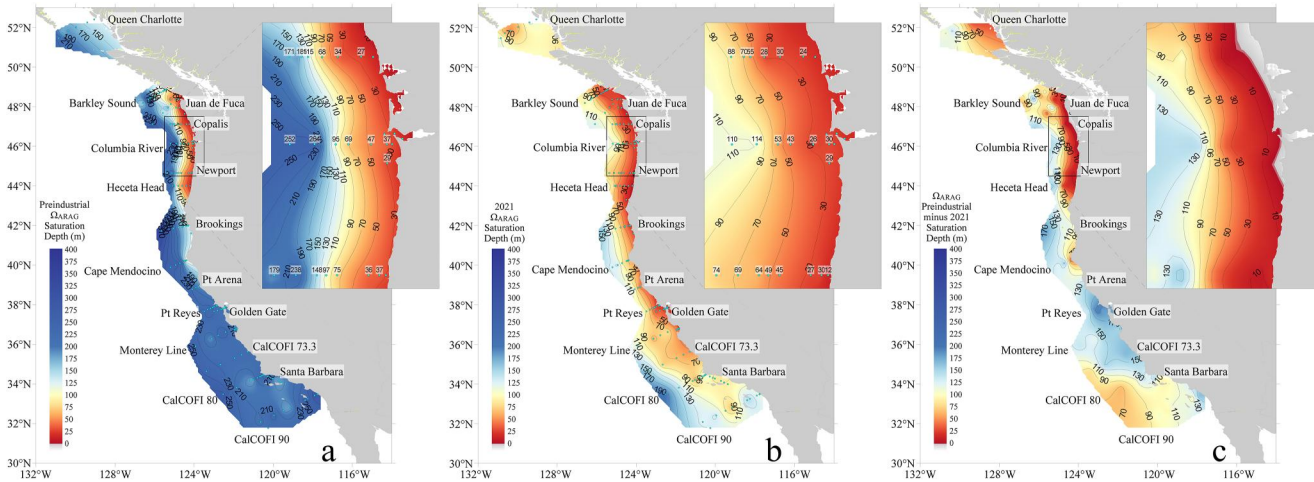

Figure 8. Plot of the aragonite saturation horizon depth along the CCE for the preindustrial condition (a) and for 2021 (b), along with the differences (in meters) between the two plots (pre-industrial – 2021; (c), indicating habitat compression due to aragonite saturation shoaling.

Within the CCE, the aragonite saturation state rates of change in surface waters are significantly lower than what is observed in the higher buffer capacity regions (−0.005 to −0.007 per yr^{-1} compared with −0.008 to −0.020 per yr^{-1}) in the subtropical regions in the Western Pacific at comparable latitudes (Table 4). This is primarily due to the lower buffer capacity of the coastal waters in CCE, which causes slower rate of change in aragonite saturation state for a given amount of DIC increase (Feely et al., 2018).

In the subsurface waters of the CCE, the most undersaturated waters with respect to aragonite occur in the nearshore bottom waters within about 5–30 km of the coast. The uptake of the preformed C_{anth} and respiration processes combine there to cause the aragonite saturation horizon to rise as much as 30–50 m since the beginning of the preindustrial era (Feely et al., 2008; Gruber et al., 2012; Turi et al., 2016) but the rates of aragonite saturation change at depths below 200 m are about half of what they are at the surface. Nevertheless, in the northern CCE, the bottom-water Ω_{ar} values are often below threshold values for dissolution and survival of pteropods and other calcifying species during the late summer and early fall months (Bednaršek et al., 2014, 2019, 2020, 2021; Feely et al., 2016). Aragonite saturation horizon depth along the CCE for the preindustrial condition are presented (Figure 8a) and for 2021 (Figure 8b), along with the differences (in meters) between the two plots (pre-industrial – 2021; Figure 8c). The difference plot represents the shoaling of the aragonite saturation horizon due to the combined effects of anthropogenic CO_2 uptake and respiration, which is, effectively, the habitat compression due to coastal acidification. The most extensive shoaling occurs on either side of the shelfbreak, where the upwelling processes are strongest. Consequently, many of the strongest impacts of ocean acidification might be expected to be observed immediately around the 2021 aragonite saturation horizon within the boundaries of the CCE.

For each biological process, the difference between the critical oxygen concentration in 2021 compared with the preindustrial period increases with the higher aragonite saturation state or pH. Consequently, as the amount and extent of acidification continues to grow larger we may expect to observe more frequent occurrences and durations of the early-stage impacts of acidification for some of the calcifying species (pteropods, decapods, and echinoderms) as their suitable habitats related to simultaneously reduced pH, Ω_{ar}, and DO undergo compression over time, which can additionally induce non-linear biological impacts, potentially restructuring vertical food-webs, and carbon export.

5. Conclusions

The California Current System is a region that is highly sensitive to the changing physical and chemical conditions associated with ocean acidification. Our results suggest that large-scale increases in C_{anth} concentrations and subsequent declines in pH and the aragonite saturation states are trending toward increased incidences of negative biological impacts for variety of different calcifying and non-calcifying marine organisms, primarily in the coastal waters where the combined effects of C_{anth} uptake, coastal upwelling, and enhanced productivity co-occur.

Because of the strong relationship between calcium carbonate saturation state and dissolved oxygen, biological thresholds will be crossed at higher oxygen concentrations in comparison with preindustrial times. The capacity of these species to acclimatize and adapt to OA, amid concurrent changes in dissolved oxygen and other drivers, which generally lags behind corresponding increases in C_{anth}, remains largely unknown. Nevertheless, the results shown here clearly indicate that the rates of acidification are increasing throughout the Pacific and that humankind may already be having a significant impact on species that play a vital role in this large and important marine ecosystem.

Data Availability Statement

The NOAA West Coast ship survey cruise physical and biogeochemical based data described in this paper are available from the NOAA National Centers for Environmental Information World Ocean Database (https://www.ncei.noaa.gov/access/ocean-carbon-acidification-data-%20system/oceans/Coastal/WCOA.html, NCEI DOIs: https://doi.org/10.25921/tzxh-n954, https://doi.org/10.7289/v5v40shg, https://doi.org/10.7289/v5c53hxp, https://doi.org/10.25921/e7m6-gh32, https://doi.org/10.7289/v5jq0xz1, https://doi.org/10.3334/cdiac/otg.clivar_nacp_west_coast_cruise_2007) and were assembled, thoroughly quality controlled, calibrated and analyzed as part of the NOAA Ocean Acidification Program.

Acknowledgments
The National Oceanic and Atmospheric Administration (NOAA) and the National Science Foundation sponsored this work. We specifically thank Libby Jewett and Dwight Gledhill of the NOAA Ocean Acidification Program and Kimberly Puglise of the NOAA National Centers for Coastal Ocean Science (Contract Number NA22NOS4780171) for their support. Nina Bednaršek was supported by the NOAA Pacific Marine Environmental Laboratory, the NOAA Ocean Acidification Program, and the Slovenian Research Agency (Project No. J12468 and No. N1-0359). This is PMEL contribution number 5422. The authors also thank Andrea Fassbender, Mar Arroyo and Michelle McClure for providing helpful suggestions for improving the manuscript.

References

Alin, S., Sutton, A., Newton, J., Mickett, J., Musielewicz, S., Curry, B., & Sabine, C. (2021). *Ocean and atmospheric CO_2*. In J. Apple, R. Wold, K. Stark, J. Bos, P. Williams, N. Hamel, et al. (Eds.), *PSEMP Marine Waters Workgroup. 2021. Puget Sound marine waters: 2020 overview*. Retrieved from www.psp.wa.gov/PSmarinewatersoverview.php

Anderson, L. A., & Sarmiento, J. L. (1994). Redfield ratios of remineralization determined by nutrient data analysis. *Global Biogeochemical Cycles*, *8*(1), 65–80. https://doi.org/10.1029/93GB03318

Arroyo, M. C., Fassbender, A. J., Carter, B. R., Edwards, C. A., Fiechter, J., Norgaard, A., & Feely, R. A. (2022). Dissimilar sensitivities of ocean acidification metrics to anthropogenic carbon accumulation in the central North Pacific Ocean and California Current Large Marine Ecosystem. *Geophysical Research Letters*, *49*(15), e2022GL097835. https://doi.org/10.1029/2022GL097835

Bates, N., Astor, Y., Church, M., Currie, K., Dore, J., González-Dávila, M., et al. (2014). A time-series view of changing ocean chemistry due to ocean uptake of anthropogenic CO_2 and ocean acidification. *Oceanography*, *27*(1), 126–141. https://doi.org/10.5670/oceanog.2014.16

Bednaršek, N., Carter, B. R., McCabe, R. M., Feely, R. A., Howard, E., Chavez, F. P., et al. (2022). Pelagic calcifiers face increased mortality and habitat loss with warming and ocean acidification. *Ecological Applications*, *32*(7), e2674. https://doi.org/10.1002/eap.2674

Bednaršek, N., Feely, R. A., Beck, M. W., Alin, S. R., Siedlecki, S. A., Calosi, P., et al. (2020). Exoskeleton dissolution with mechanoreceptor damage in larval Dungeness crab related to severity of present-day ocean acidification vertical gradients. *The Science of the Total Environment*, *716*, 136610. https://doi.org/10.1016/j.scitotenv.2020.136610

Bednaršek, N., Feely, R. A., Howes, E. L., Hunt, B. P. V., Kessouri, F., León, P., et al. (2019). Systematic review and meta-analysis towards synthesis of thresholds of ocean acidification impacts on calcifying pteropods and interactions with warming. *Frontiers in Marine Science*, *6*, 227. https://doi.org/10.3389/fmars.2019.00227

Bednaršek, N., Feely, R. A., Reum, J. C. P., Peterson, W., Menkel, J., Alin, S. R., & Hales, B. (2014). *Limacina helicina* shell dissolution as an indicator of declining habitat suitability due to ocean acidification in the California Current Ecosystem. *Proceedings of the Royal Society B*, *281*(1785), 20140123. https://doi.org/10.1098/rspb.2014.0123

Bednaršek, N., Naish, K. A., Feely, R. A., Hauri, C., Kimoto, K., Hermann, A. J., et al. (2021). Integrated assessment of ocean acidification risks to pteropods in the northern high latitudes: Regional comparison of exposure, sensitivity and adaptive capacity. *Frontiers in Marine Science*, *8*, 671497. https://doi.org/10.3389/fmars.2021.671497

Bednaršek, N., Tarling, G. A., Bakker, D. C., Fielding, S., Cohen, A., Kuzirian, A., et al. (2012). Description and quantification of pteropod shell dissolution: A sensitive bioindicator of ocean acidification. *Global Change Biology*, *18*(7), 2378–2388. https://doi.org/10.1111/j.1365-2486.2012.02668.x

Booth, A. T., McPhee, E. E., Chua, P., Kingsley, E., Denny, M., Phillips, R., et al. (2012). Natural intrusions of hypoxic, low pH water into nearshore marine environments on the California coast. *Continental Shelf Research*, *45*, 108–115. https://doi.org/10.1016/j.csr.2012.06.009

Byrne, R. H., Mecking, S., Feely, R. A., & Liu, X. (2010). Direct observations of basin-wide acidification of the North Pacific Ocean. *Geophysical Research Letters*, *37*(2), L02601. https://doi.org/10.1029/2009GL040999

Caldeira, K., & Wickett, M. E. (2003). Anthropogenic carbon and ocean pH. *Nature*, *425*(6956), 365. https://doi.org/10.1038/425365a

Carpenter, J. H. (1965). The Chesapeake Bay Institute technique for the Winkler dissolved oxygen method. *Limnology & Oceanography*, *10*(1), 141–143. https://doi.org/10.4319/lo.1965.10.1.0141

Carter, B. R., Feely, R. A., Mecking, S., Cross, J. N., Macdonald, A. M., Siedlecki, S. A., et al. (2017). Two decades of Pacific anthropogenic carbon storage and ocean acidification along Global Ocean Ship-based Hydrographic Investigations Program sections P16 and P02. *Global Biogeochemical Cycles*, *31*(2), 306–327. https://doi.org/10.1002/2016GB005485

Carter, B. R., Feely, R. A., Wanninkhof, R., Kouketsu, S., Sonnerup, R. E., Pardo, P. C., et al. (2019). Pacific anthropogenic carbon between 1991 and 2017. *Global Biogeochemical Cycles*, *33*(5), 597–617. https://doi.org/10.1029/2018GB006154

Chan, F., Barth, J. A., Blanchette, C. A., Byrne, R. H., Chavez, F., Cheriton, O., et al. (2017). Persistent spatial structuring of coastal ocean acidification in the California Current System. *Scientific Reports*, *7*(1), 2526. https://doi.org/10.1038/s41598-017-02777-y

Chavez, F. P., Pennington, J. T., Michisaki, R. P., Blum, M., Chavez, G. M., Friederich, J., et al. (2017). Climate variability and change: Response of a coastal ocean ecosystem. *Oceanography*, *30*(4), 128–145. https://doi.org/10.5670/oceanog.2017.429

Desmet, F., Gruber, N., Köhn, E. E., Münnich, M., & Vogt, M. (2022). Tracking the space-time evolution of ocean acidification extremes in the California current system and northeast Pacific. *Journal of Geophysical Research: Oceans*, *127*(5), e2021JC018159. https://doi.org/10.1029/2021JC018159

Dickson, A. G. (1990). Thermodynamics of the dissociation of boric acid in synthetic seawater from 273.15 to 298.25 K. *Deep-Sea Research*, *37*(5), 755–766. https://doi.org/10.1016/0198-0149(90)90004-f

DOE. (1994). *Handbook of Methods for the Analysis of the Various Parameters of the Carbon Dioxide System in Sea Water, Version 2 (ORNL/CDIAC-74)*. US Department of Energy.

Doney, S. C., Balch, W. M., Fabry, V. J., & Feely, R. A. (2009). Ocean acidification: A critical emerging problem for the ocean sciences. *Oceanography*, *22*(4), 18–27. https://doi.org/10.5670/oceanog.2009.93

Doney, S. C., Busch, D. S., Cooley, S. R., & Kroeker, K. J. (2020). The impacts of ocean acidification on marine ecosystems and reliant human communities. *Annual Review of Environment and Resources*, *45*(1), 83–112. https://doi.org/10.1146/annurev-environ-012320-083019

Egleston, E. S., Sabine, C. L., & Morel, F. M. M. (2010). Revelle revisited: Buffer factors that quantify the response of ocean chemistry to changes in DIC and alkalinity. *Global Biogeochemical Cycles*, *24*(1), GB1002. https://doi.org/10.1029/2008GB003407

Ekstrom, J. A., Suatoni, L., Cooley, S. R., Pendleton, L. H., Waldbusser, G. G., Cinner, J. E., et al. (2015). Vulnerability and adaptation of US shellfisheries to ocean acidification. *Nature Climate Change*, *5*(3), 207–214. https://doi.org/10.1038/NCLIMATE2508

Engström-Öst, J., Glippa, O., Feely, R. A., Kanerva, M., Keister, J. E., Alin, S. R., et al. (2019). Eco-physiological responses of copepods and pteropods to ocean warming and acidification. *Scientific Reports*, *9*(1), 4748. https://doi.org/10.1038/s41598-019-41213-1

Evans, W., Hales, B., & Strutton, P. G. (2013). pCO_2 distributions and air-water CO_2 fluxes in the Columbia River estuary. *Estuarine, Coastal and Shelf Science*, *117*, 260–272. https://doi.org/10.1016/j.ecss.2012.12.003

Fassbender, A. J., Rodgers, K. B., Palevsky, H. I., & Sabine, C. L. (2018). Seasonal asymmetry in the evolution of surface ocean pCO_2 and pH thermodynamic drivers and the influence on sea-air CO_2 flux. *Global Biogeochemical Cycles*, *32*(10), 1476–1497. https://doi.org/10.1029/2017GB005855

Fassbender, A. J., Sabine, C. L., Feely, R. A., Langdon, C., & Mordy, C. W. (2011). Inorganic carbon dynamics during northern California coastal upwelling. *Continental Shelf Research*, *31*(11), 1180–1192. https://doi.org/10.1016/j.csr.2011.04.006

Feely, R. A., Alin, S., Carter, B., Bednaršek, N., Hales, B., Chan, F., et al. (2016). Chemical and biological impacts of ocean acidification along the west coast of North America. *Estuarine, Coastal and Shelf Science*, *183*(A), 260–270. https://doi.org/10.1016/j.ecss.2016.08.043

Feely, R. A., Doney, S. C., & Cooley, S. R. (2009). Ocean acidification: Present conditions and future changes in a high-CO_2 world. *Oceanography*, *22*(4), 36–47. https://doi.org/10.5670/oceanog.2009.95

Feely, R. A., Okazaki, R. R., Cai, W.-J., Bednaršek, N., Alin, S. R., Byrne, R. H., & Fassbender, A. (2018). The combined effects of acidification and hypoxia on pH and aragonite saturation in the coastal waters of the Californian Current Ecosystem and the northern Gulf of Mexico. *Continental Shelf Research*, *152*, 50–60. https://doi.org/10.1016/j.csr.2017.11.002

Feely, R. A., Sabine, C. L., Hernandez-Ayon, J. M., Ianson, D., & Hales, B. (2008). Evidence for upwelling of corrosive "acidified" water onto the Continental Shelf. *Science*, *320*(5882), 1490–1492. https://doi.org/10.1126/science.1155676

Franco, A. C., Ianson, D., Ross, T., Hamme, R. C., Monahan, A. H., Christian, J. R., et al. (2021). Anthropogenic and climatic contributions to observed carbon system trends in the northeast Pacific. *Global Biogeochemical Cycles*, *35*(7), e2020GB006829. https://doi.org/10.1029/2020gb006829

Frieder, C. A., Gonzalez, J. P., Bockmon, E. E., Navarro, M. O., & Levin, L. A. (2014). Can variable pH and low oxygen moderate ocean acidification outcomes for mussel larvae? *Global Change Biology*, *20*(3), 754–764. https://doi.org/10.1111/gcb.12485

Friedlingstein, P., Jones, M. W., O'Sullivan, M., Andrew, R. M., Bakker, D. C. E., Hauck, J., et al. (2022). Global carbon Budget 2021. *Earth System Science Data*, *14*(4), 1917–2005. https://doi.org/10.5194/essd-14-1917-2022

Friedlingstein, P., O'Sullivan, M., Jones, M. W., Andrew, R. M., Hauck, J., Olsen, A., et al. (2020). Global Carbon Budget 2020. *Earth System Science Data*, *12*(4), 3269–3340. https://doi.org/10.5194/essd-12-3269-2020

Friis, K., Kortzinger, A., Patsch, J., & Wallace, D. W. R. (2005). On the temporal increase of anthropogenic CO_2 in the subpolar North Atlantic. *Deep-Sea Research Part I*, *52*(5), 681–698. https://doi.org/10.1016/j.dsr.2004.11.017

Gattuso, J.-P., Magnan, A., Billé, R., Cheung, W. W. L., Howes, E., Joos, F., et al. (2015). Contrasting futures for ocean and society from different anthropogenic CO_2 emissions scenarios. *Science*, *349*(6243), aac4722. https://doi.org/10.1126/science.aac4722

Gobler, C. J., & Baumann, H. (2016). Hypoxia and acidification in ocean ecosystems: Coupled dynamics and effects on marine life. *Biology Letters*, *12*(5), 20150976. https://doi.org/10.1098/rsbl.2015.0976

Grantham, B. A., Chan, F., Nielsen, K. J., Fox, D. S., Barth, J. A., Lubchenco, J., & Menge, B. A. (2004). Upwelling-driven nearshore hypoxia signals ecosystem and oceanographic changes in the northeast Pacific. *Nature*, *429*(6993), 749–754. https://doi.org/10.1038/nature02605

Gruber, N., Clement, D., Carter, B. R., Feely, R. A., van Heuven, S., Hoppema, M., et al. (2019). The oceanic sink for anthropogenic CO_2 from 1994 to 2007. *Science*, *363*(6432), 1193–1199. https://doi.org/10.1126/science.aau5153

Gruber, N., Hauri, C., Lachkar, Z., Loher, D., Frölicher, T. L., & Plattner, G.-K. (2012). Rapid progression of ocean acidification in the California Current System. *Science*, *337*(6091), 220–223. https://doi.org/10.1126/science.1216773

Hales, B., Karp-Boss, L., Perlin, A., & Wheeler, P. (2006). Oxygen production and carbon sequestration in an upwelling coastal margin. *Global Biogeochemical Cycles*, *20*(3), GB3001. https://doi.org/10.1029/2005GB002517

Hales, B., Takahashi, T., & Bandstra, L. (2005). Atmospheric CO_2 uptake by a coastal upwelling system. *Global Biogeochemical Cycles*, *19*(1), GB1009. https://doi.org/10.1029/2004GB002295

Harris, K. E., DeGrandpre, M. D., & Hales, B. (2013). Aragonite saturation state dynamics in a coastal upwelling zone. *Geophysical Research Letters*, *40*(11), 2720–2725. https://doi.org/10.1002/grl.50460

Hauri, C., Gruber, N., Vogt, M., Doney, S. C., Feely, R. A., Lachkar, Z., et al. (2013). Spatiotemporal variability and long-term trends of ocean acidification in the California Current System. *Biogeosciences*, *10*(1), 193–216. https://doi.org/10.5194/bg-10-193-2013

IPCC. (2013). *Climate Change 2013: The Physical Science Basis. Contributions of Working Group I to the Fifth Assessment Report of the Intergovernmental Panel on Climate Change*. In T. F. Stocker, D. Qin, G. –K. Plattner, M. Tignor, S. K. Allen, et al. (Eds.), Cambridge University Press.

Ishii, M., Kosugi, N., Sasano, D., Saito, S., Midorikawa, T., & Inoue, H. Y. (2011). Ocean acidification off the south coast of Japan: A result from time series observations of CO_2 parameters from 1994 to 2008. *Journal of Geophysical Research*, *116*(C6), C06022. https://doi.org/10.1029/2010JC006831

Ishii, M., Rodgers, K. B., Inoue, H. Y., Toyama, K., Sasano, D., Kosugi, N., et al. (2020). Ocean acidification from below in the tropical Pacific. *Global Biogeochemical Cycles*, *34*(8), e2019GB006368. https://doi.org/10.1029/2019GB006368

Jiang, L.-Q., Carter, B. R., Feely, R. A., Lauvset, S. K., & Olsen, A. (2019). Surface ocean pH and buffer capacity: Past, present and future. *Scientific Reports*, *9*(1), 18624. https://doi.org/10.1038/s41598-019-55039-4

Johnson, K. M., Sieburth, J. M., Williams, P. J. L., & Brändström, L. (1987). Coulometric total carbon dioxide analysis for marine studies: Automation and calibration. *Marine Chemistry*, *21*(2), 117–133. https://doi.org/10.1016/0304-4203(87)90033-8

Jones, C., Robertson, E., Arora, V., Friedlingstein, P., Shevliakova, E., Bopp, L., et al. (2013). Twenty-first-century compatible CO_2 emissions and airborne fraction simulated by CMIP Earth system models under four representative concentration pathways. *Journal of Climate*, *26*(13), 4398–4413. https://doi.org/10.1175/jcli-d-12-00554.1

Joos, F., Frölicher, T. L., Steinacher, M., & Plattner, G.-K. (2011). *Impact of climate change mitigation on ocean acidification projections*. In J.-P. Gattuso & L. Hansson (Eds.), *Ocean acidification* (pp. 272–290). Oxford University Press.

Kwiatkowski, L., & Orr, J. C. (2018). Diverging seasonal extremes for ocean acidification during the twenty-first century. *Nature Climate Change*, *8*(2), 141–145. https://doi.org/10.1038/s41558-017-0054-0

Laruelle, G. G., Cai, W.-J., Hu, X., Gruber, N., Mackenzie, F. T., & Regnier, P. (2018). Continental shelves as a variable but increasing global sink for atmospheric carbon dioxide. *Nature Communications*, *9*(1), 454. https://doi.org/10.1038/s41467-017-02738-z

Lauvset, S. K., Gruber, N., Landschützer, P., Olsen, A., & Tjiputra, J. (2015). Trends and drivers in global surface ocean pH over the past 3 decades. *Biogeosciences*, *12*(5), 1285–1298. https://doi.org/10.5194/bg-12-1285-2015

Lee, K., Kim, T.-W., Byrne, R. H., Millero, F. J., Feely, R. A., & Liu, Y.-M. (2010). The universal ratio of boron to chlorinity for the North Pacific and North Atlantic oceans. *Geochimica et Cosmochimica Acta*, *74*(6), 1801–1811. https://doi.org/10.1016/j.gca.2009.12.027

Lewis, E., & Wallace, D. W. R. (1998). *Program developed for CO2 system calculations*. In *ORNL/CDIAC-105, Carbon Dioxide Information Analysis Center*. Oak Ridge National Laboratory. Available online at http://cdiac.ornl.gov/ftp/co2sys/CO2SYS_calc_DOS_v1.05/cdiac105.pdf

Lida, Y., Takatani, Y., Kojima, A., & Ishii, M. (2020). Global trends of ocean CO_2 sink and ocean acidification: An observation-based reconstruction of surface ocean inorganic carbon variables. *Journal of Oceanography*, *77*, 325–358. https://doi.org/10.1007/s10872-020-00571-5

Lueker, T. J., Dickson, A. G., & Keeling, C. D. (2000). Ocean pCO_2 calculated from dissolved inorganic carbon, alkalinity, and equations for K_1 and K_2: Validation based on laboratory measurements of CO_2 in gas and seawater at equilibrium. *Marine Chemistry*, *70*(1–3), 105–119. https://doi.org/10.1016/s0304-4203(00)00022-0

Mekkes, L., Renema, W., Bednaršek, N., Alin, S. R., Feely, R. A., Huisman, J., et al. (2021). Pteropods make thinner shells in the upwelling region of the California Current Ecosystem. *Scientific Reports*, *11*(1), 1731. https://doi.org/10.1038/s41598-021-81131-9

Millero, F. J. (1995). Thermodynamics of the carbon-dioxide system in the oceans. *Geochimica et Cosmochimica Acta*, *59*(4), 661–677. https://doi.org/10.1016/0016-7037(94)00354-o

Millero, F. J., Zhang, J. Z., Lee, K., & Campbell, D. M. (1993). Titration alkalinity of seawater. *Marine Chemistry*, *44*(2–4), 153–165. https://doi.org/10.1016/0304-4203(93)90200-8

Mucci, A. (1983). The solubility of calcite and aragonite in seawater at various salinities, temperatures, and one atmosphere total pressure. *American Journal of Science*, *283*(7), 780–799. https://doi.org/10.2475/ajs.283.7.780

Ono, H., Kosugi, N., Toyama, K., Tsujino, H., Kojima, A., Enyo, K., et al. (2019). Acceleration of ocean acidification in the Western North Pacific. *Geophysical Research Letters*, *46*(22), 13161–13169. https://doi.org/10.1029/2019GL085121

Ono, T., Watanabe, S., Okuda, K., & Fukasawa, M. (1998). Distribution of total carbonate and related properties in the North Pacific along 30°N. *Journal of Geophysical Research: Oceans*, *103*(C13), 30873–30883. https://doi.org/10.1029/1998jc900018

Orr, J. C., Fabry, V. J., Aumont, O., Bopp, L., Doney, S. C., Feely, R. A., et al. (2005). Anthropogenic ocean acidification over the twenty-first century and its impact on calcifying organisms. *Nature*, *437*(7059), 681–686. https://doi.org/10.1038/nature04095

Osborne, E. B., Thunell, R. C., Gruber, N., Feely, R. A., & Benitez-Nelson, C. R. (2019). Decadal variability in twentieth-century ocean acidification in the California Current Ecosystem. *Nature Geoscience*, *13*(1), 43–49. https://doi.org/10.1038/s41561-019-0499-z

Pörtner, H. O. (2012). Integrating climate-related stressor effects on marine organisms: Unifying principles linking molecule to ecosystem-level changes. *Marine Ecology Progress Series*, *470*, 273–290. https://doi.org/10.3354/meps10123

Rykaczewski, R. R., & Dunne, J. P. (2010). Enhanced nutrient supply to the California Current Ecosystem with global warming and increased stratification in an earth system model. *Geophysical Research Letters*, *37*(21), L21606. https://doi.org/10.1029/2010GL045019

Sabine, C. L., Feely, R. A., Gruber, N., Key, R. M., Lee, K., Bullister, J. L., et al. (2004). The oceanic sink for anthropogenic CO_2. *Science*, *305*(5682), 367–371. https://doi.org/10.1126/science.1097403

Siedlecki, S. A., Kaplan, I. C., Hermann, A. J., Nguyen, T. T., Bond, N. A., Newton, J. A., et al. (2016). Experiments with seasonal forecasts of ocean conditions for the northern region of the California Current upwelling system. *Scientific Reports*, *6*(1), 27203. https://doi.org/10.1038/srep27203

Siedlecki, S. A., Pilcher, D., Howard, E. M., Deutsch, C., MacCready, P., Norton, E. L., et al. (2021). Coastal processes modify projections of some climate-driven stressors in the California Current System. *Biogeosciences*, *18*(9), 2871–2890. https://doi.org/10.5194/bg-18-2871-2021

Somero, G. N., Beers, J., Chan, F., Hill, T., Klinger, T., & Litvin, S. (2016). What changes in the carbonate system, oxygen, and temperature portend for the northeastern Pacific Ocean: A physiological perspective. *BioScience*, *66*(1), 14–26. https://doi.org/10.1093/biosci/biv162

Steinacher, M., Joos, F., Frölicher, T. L., Plattner, G.-K., & Doney, S. C. (2009). Imminent ocean acidification in the Arctic projected with the NCAR global coupled carbon cycle-climate model. *Biogeosciences*, *6*(4), 515–533. https://doi.org/10.5194/bg-6-515-2009

Sutton, A. J., Feely, R. A., Sabine, C. L., McPhaden, M. J., Takahashi, T., Chavez, F. P., et al. (2014). Natural variability and anthropogenic change in equatorial Pacific surface ocean pCO_2 and pH. *Global Biogeochemical Cycles*, *28*(2), 131–145. https://doi.org/10.1002/2013GB004679

Sutton, A. J., Wanninkhof, R., Sabine, C. L., Feely, R. A., Cronin, M. F., & Weller, R. A. (2017). Variability and trends in surface seawater pCO_2 and CO_2 flux in the Pacific Ocean. *Geophysical Research Letters*, *44*(11), 5627–5636. https://doi.org/10.1002/2017GL073814

Thomson, R. E., & Krassovski, M. V. (2010). Poleward reach of the California undercurrent extension. *Journal of Geophysical Research*, *115*(C9), C09027. https://doi.org/10.1029/2010JC006280

Turi, G., Lachkar, Z., Gruber, N., & Munnich, M. (2016). Climatic modulation of recent trends in ocean acidification in the California Current System. *Environmental Research Letters*, *11*(1), 014007. https://doi.org/10.1088/1748-9326/11/1/014007

UNESCO. (1994). *Protocols for the Joint Global Ocean Flux Study (JGOFS) Core Measurements*. United Nations Educational, Scientific, and Cultural Organization. Retrieved from http://ijgofs.whoi.edu/Publications/Report_Series/JGOFS_19.pdf

Wakita, M., Nagano, A., Fujiki, T., & Watanabe, S. (2017). Slow acidification of the winter mixed layer in the subarctic western North Pacific. *Journal of Geophysical Research: Oceans*, *122*(8), 6923–6935. https://doi.org/10.1002/2017JC013002

Waldbusser, G. G., Hales, B., Langdon, C. J., Haley, B. A., Schrader, P., Brunner, E. L., et al. (2015). Saturation state sensitivity of marine bivalve larvae to ocean acidification. *Nature Climate Change*, *5*(3), 273–280. https://doi.org/10.1038/nclimate2479

Wang, Y., Hendy, I., & Napier, T. J. (2017). Climate and anthropogenic controls of coastal deoxygenation on interannual to centennial timescales. *Geophysical Research Letters*, *44*(22), 11528–11536. https://doi.org/10.1002/2017gl075443

Wolfe, W. H., Martz, T. R., Dickson, A. G., Goericke, R., & Ohman, M. D. (2023). A 37-year record of ocean acidification in the Southern California current. *Commun Earth Environ*, *4*(1), 406. https://doi.org/10.1038/s43247-023-01065-0